Journal of Manufacturing Processes 66 (2021) 325–340

Contents lists available at ScienceDirect

Journal of Manufacturing Processes

journal homepage: www.elsevier.com/locate/manpro

Quantification of the hardness response in the heat-affected zone of low alloy steels subjected to temper bead welding

Jeffrey Stewart, Boian Alexandrov *

The Ohio State University, United States

ARTICLE INFO

Keywords:
Temper bead welding
Tempering response quantification
Low alloy steels
Heat affected zone
Weld thermal history
Carbide precipitation

ABSTRACT

The tempering response in the heat-affected zone (HAZ) of low alloy steels during temper bead welding is heavily dependent on the experienced thermal history. Past work has developed quantification approaches for isothermal tempering conditions and single non-isothermal tempering cycles, whereas the temper bead welding processes impart multiple non-isothermal cycles throughout the HAZ. This work outlines a novel methodology for tempering response quantification that allows for prediction of the HAZ hardness in multipass welding. The quantification approach utilizes a modification of the Grange-Baughman tempering parameter that converts non-isothermal cycles into an equivalent isothermal cycle and correlate this with the resulting hardness. This relationship can be utilized to evaluate hardness distributions throughout the HAZ of low alloy steel temper bead weldments based on the experienced thermal histories. It was shown that, in contrast with conventional heat treatment, the temper bead welding in Grade 22 steel results in nucleation of high density, finely dispersed Fe-Cr rich carbides.

The proposed methodology was applied for evaluation of the HAZ hardness in a particular heat of Grade 22 steel, resulting from multiple tempering reheats, and was experimentally validated using a three-layer weld overlay. It was found that the peak temperature of weld tempering cycles was the most significant factor in controlling HAZ hardness.

1. Introduction

Low allow steels are among the most widely used structural mater-Sials in the world. A common concern when fabricating welded structures from low alloy steels is the formation of hard martensitic microstructure in the heat affected zone (HAZ) that leads to loss of toughness and increased susceptibility to hydrogen-assisted cracking (HAC), as pointed out by Smith [1]. A post-weld heat treatment (PWHT) is often performed to improve toughness and reduce hardness, by tempering the martensitic microstructure, and to relieve residual stress imparted by the welding process.

Grade 22 steel contains nominally 2.25 wt% Cr and 1% Mo and is classified as a creep-resistant steel. Steels from this class possess improved creep and toughness properties due to the formation of complex alloy carbides during tempering. Such steels are typically used in applications where high temperature performance is required, such as in the oil & gas and power generation industries. The mechanisms of carbides formation in creepresistant steels and their effect on mechanical properties and service performance have been thoroughly investigated. Porter and Easterling [2] explain that the supersaturation of martensite with carbon provides sufficient activation energy for precipitation of carbides during tempering. They specify two mechanisms of alloyed carbides formation: 1) from already precipitated cementite and 2) through heterogeneous nucleation at dislocations, lath boundaries, and prior austenite grain boundaries. Baker and Nutting [3] developed the first time-temperature transformation diagram for carbide precipitation in Grade 22 steel. They proposed the following sequence of precipitation as the temperature and time of heat treatment increase within the typical ranges of heat treatment: ε-carbide + M_3C; M_3C; M_3C + M_2C + M_7C_3; M_2C + M_7C_3. According to their diagram, $M_{23}C_6$ and M_6C can form during longer duration exposures at higher temperatures related to service. Yu [4] investigated the effects of P, Si and Mn on carbide precipitation in Grade 22 steel. He found out that Mn accelerates formation of M_7C_3, while Si changes the precipitation sequence accelerating precipitation of Mo rich M_2C and allowing formation of M_6C. Dépinoy et al. [5] studied the tempering behavior in Grade 22 steel using thermodynamic simulations and transmission electron microscopy. They identified $M_{23}C_6$ as a stable carbide that forms from dissolving M_3C carbides in

* Corresponding author at: 1248 Arthur E Adams Dr., Columbus, OH, 43221, United States.
E-mail address: Alexandrov.1@osu.edu (B. Alexandrov).

https://doi.org/10.1016/j.jmapro.2021.04.008
Received 6 February 2021; Received in revised form 4 April 2021; Accepted 7 April 2021
Available online 20 April 2021

the early stages of heat treatment and from M_7C_3 at longer holding times. The softening kinetics of the material was related to the precipitation and coarsening of $M_{23}C_6$. The absence of secondary hardening effects was attributed to the stable behavior of M_2C and to M_6C not forming in the studied conditions of heat treatment. Parameswaran et al. [6] found that precipitation of semi-coherent M_2C carbides leads to secondary hardening, while formation of incoherent M_7C_3 and $M_{23}C_6$ results in softening. Although the precipitation behavior of Grade 22 steel is well understood, quantitative relationships of the type and phase fraction of carbides to the hardness reduction, resulting from heat treatment, have not been established yet.

There have been many attempts for quantification of the tempering response in steels and for development of useful relationships for selection of optimal heat treatment temperatures and durations. In general, the existing heat treatment procedures can be classified into two main types: isothermal and non-isothermal. Isothermal tempering is performed at constant temperature for a prescribed duration. The majority of traditional tempering procedures fall under this category and involve durations on the order of hours. The first major work on quantification of the tempering response in steels during isothermal heat treatment was performed by Hollomon and Jaffe [7]. They studied heat treatment temperatures ranging from 100 °C to 700 °C and durations from 10 s to 24 h on low alloy steels with carbon contents between 0.31 and 1.15 wt% C. Under the assumption that the hardness evolution during tempering was primarily a function of diffusion, they derived an equation that allowed tempering duration and temperature to be combined into a single parameter:

$$HJP = T*(C + \log(t)) \tag{1}$$

where HJP is the Hollomon-Jaffe parameter, T is the tempering temperature in degrees Kelvin, t is the tempering duration in hours, and C is a material dependent constant that can be determined experimentally. Andrews [8] has pointed out that the tempering temperature in the Hollomon-Jaffe equation has much stronger effect on the resulting hardness than the tempering duration. In a study on AISI 4340 steel, Nehrenberg [9] showed that the Hollomon-Jaffe equation can be used for quantification of tempering that is carried out in multiple thermal cycles at the same tempering temperature. He also suggested that the tempering parameters should be additive, even if conducted at different temperatures.

Hollomon and Jaffe [7] recommended C values between 15 and 19.5 based on the carbon content of steels being tempered. Grange and Baughman [10] have shown that the exact value of C is not critical and a value of 18 is satisfactory for a range of carbon and alloy steels. This was demonstrated in series of hardness plots based on a modified Hollomon-Jaffe relationship:

$$GBP = T*(18 + \log(t)) \tag{2}$$

where T is the tempering temperature in degrees Rankine, $T(^oR) = T(K)$ x 9/5.

Grange and Baughman [10] and Grange at al [11]. studied alloyed steels with the intention of quantifying the effects of individual alloying elements on hardness after tempering. They found that alloying additions slowed the reduction in hardness during tempering, quantified the contribution of alloying elements, and suggested an additive equation for hardness estimation:

$$Hardness = HV + \Delta HV_{Mn} + \Delta HV_P + \Delta HV_{Si} + \Delta HV_{Ni} + \Delta HV_{Cr} + \Delta HV_V \tag{3}$$

where HV is the hardness of a corresponding carbon steel and the subsequent ΔHV terms are correction factors for alloying elements. The correction factors were found to be dependent on both the GBP value and the alloying content.

Non-isothermal tempering refers to thermal cycles that exhibit temperature variations rather than maintaining a constant holding temperature. There are many applications where a component experiences non-isothermal tempering cycles, including but not limited to induction tempering, spot heat treatment, temper bead welding, multi-pass welding, additive manufacturing. Semiatin et al. [12] applied the Grange Baughman relationship, Eq. (4), to develop an "effective tempering parameter" that can be used for the quantification of short-time induction heat treatments:

$$GBP = T*(14.44 + \log(t)) \tag{4}$$

where GBP is a Grange-Baughman type parameter, T is the tempering temperature in degrees Rankine, t is the tempering time in seconds.

The non-isothermal cycle is split into small segments, as shown in Fig. 1. Each segment is treated as a small isothermal cycle and has an associated GBP value based on the average temperature over that segment, T_i, and the time length of the segment, Δt_i. The GBP_i value is used to calculate the holding time Δt_i^* of an equivalent tempering cycle with holding temperature T^* that is the peak temperature of the non-isothermal cycle. The calculation procedure utilizes Eqs. (5)–(7), and is demonstrated in Fig. 2.

$$GBP_i = T_i(14.44 + \log(\Delta t_i)) \tag{5}$$

$$GBP_i = T^*\left(14.44 + \log\left(\Delta t_i^*\right)\right) \tag{6}$$

$$\Delta t_i^* = 10^{\left[\frac{T_i}{T^*}(14.44+\log(\Delta t_i))-14.44\right]} \tag{7}$$

All Δt_i^* values are added together to generate the equivalent holding time t^* of an isothermal cycle with peak temperature T^*, as shown in Fig. 3. The parameters of this isothermal cycle (t^* and T^*) are then used to calculate a GBP parameter that would represent the tempering effect of the non-isothermal cycle, Eq. (4). This approach and its application to induction tempering are detailed by Semiatin et al. [13].

With the development of more powerful computing capabilities in recent years, there have been efforts to utilize artificial neural networks (ANNs) for quantification of non-isothermal tempering cycles. Yu et al. [14] developed a neural network in conjunction with a "thermal cycle tempering parameter" (TCTP) that is similar to the effective tempering parameter developed by Semiatin et al. [12]. The ANN is built by

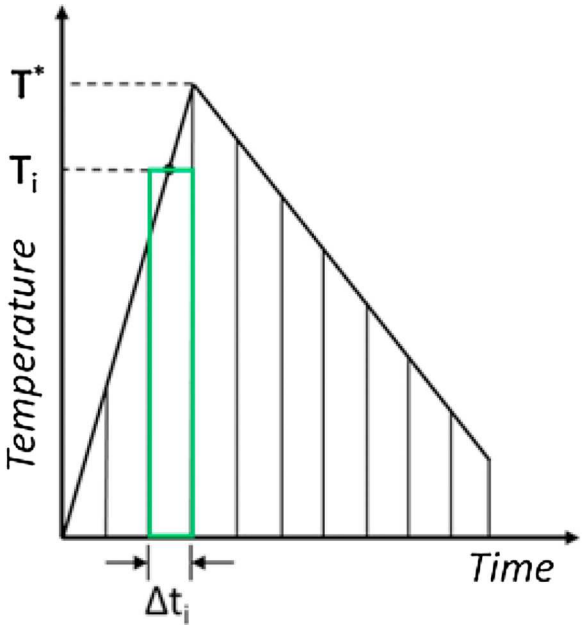

Fig. 1. Division of non-isothermal cycle into isothermal sections, Semiatin et al. [12].

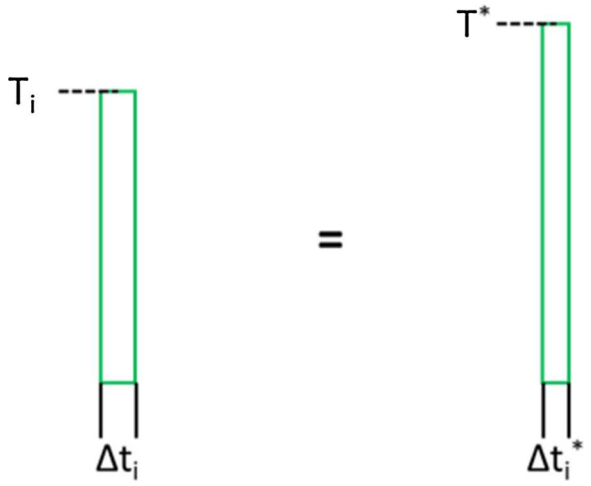

Fig. 2. Equivalency of GBPi and GBPi* used to calculate Δt_i^* values for each isothermal division, Semiatin et al. [12].

providing training data and allowing the model to identify relationships between inputs and outputs. In the case of Yu's work, there were three inputs: the TCTP value, the peak temperature of the thermal cycle, and the cooling rate of the thermal cycle. The output was hardness. Using this ANN, Yu was able to predict hardness values very accurately in the HAZ of several temper bead samples. However, building ANN models requires significant amount of training data. For example, the neural network built by Yu et al. required 500 hardness data sets to characterize one alloy. In a follow-up publication, Yu et al. [15] utilized the TCTP parameter for quantification of the effect of heating and cooling rates on tempering during conventional PWHT. They demonstrated that typical PWHT heating and cooling rates, in the range of 10 °C/h to 200 °C/h, have significant contribution to the overall hardness reduction, while the effect of holding time at PWHT temperature is insignificant.

Temper bead welding (TBW) is often used in situations where PWHT is too time consuming, expensive, or impractical, such as in the repair of large components or complex welded structures. TBW refers to welding processes that utilize the heat input from adjacent weld passes and subsequent weld layers to provide tempering in the base metal or weld metal HAZ, Sperko [16]. In order for tempering to occur, the peak temperatures generated from adjacent passes and subsequent layers must be high enough to temper the undelaying HAZ but should not exceed the A_{C1} temperature. In case the A_{C1} temperature is exceeded, fresh martensite will form upon cooling and any tempering that has occurred up to that point will be lost. Wang et al. [17] noted that the effectiveness of a temper bead welding procedure depends on many factors, including materials composition, welding process, heat input, travel speed, bead geometry, bead overlap, and preheat/interpass temperature.

Various industry standards and codes address the development and implementation of TBW procedures. The ASME Boiler and Pressure Vessel Code (BPVC) Section IX (QW-290) outlines specific requirements for qualification of temper bead procedures and identifies the bead placement, overlap, welding process, and heat input as essential variables for the process. TBW procedures are qualified by hardness testing or impact testing. Several other codes and standards, including AWS, API, and the Canadian Standards Association (CSA) allow for the use of temper bead techniques, referring to ASME BPVC Section IX and multiple ASME code cases for procedure qualification. TBW procedures for use in the nuclear power industry are regulated by the National Board Inspection Code (NBIC). The Welding Research Council supported an extensive research effort, performed by Wang 2006, in development of the so-called half-bead temper-bead controlled deposition techniques, where weld beads are partially removed to allow HAZ tempering by subsequent weld beads.

Most TBW procedures currently used in industry are developed using trial and error approaches and require significant time and resources for development and qualification. Designing a procedure that meets relevant acceptance criteria can lead to a large number of test coupons being generated, and often the impact that certain process parameters have on the resulting hardness is not fully understood. Boring [18] demonstrated the complexity in TBW procedure development for in-service repair of an amine tower. Four different procedures were tested and failed to meet a maximum hardness criterion of 200 HV required by NBIC and ASME codes. Bead placement optimization in one of the procedures was needed to avoid hard spots at weld toes and produce acceptable welds. Peterson [19] described two failed attempts to meet relevant ASME acceptance criteria in the development and qualification of a TBW procedure for repair of 0.5Cr-0.5Mo steel used in nuclear power plants. TBW procedures that have been qualified and used in industry in the past can still require update qualification efforts if acceptance criteria are added for an application. The impacts that specific process parameters have on the resulting HAZ properties are multifaceted and can lead to significant resource expenditures on development and qualification of acceptable temper bead welding procedures.

The objective of this study was to develop a methodology for quantification of tempering response in steels subjected to multipass welding,

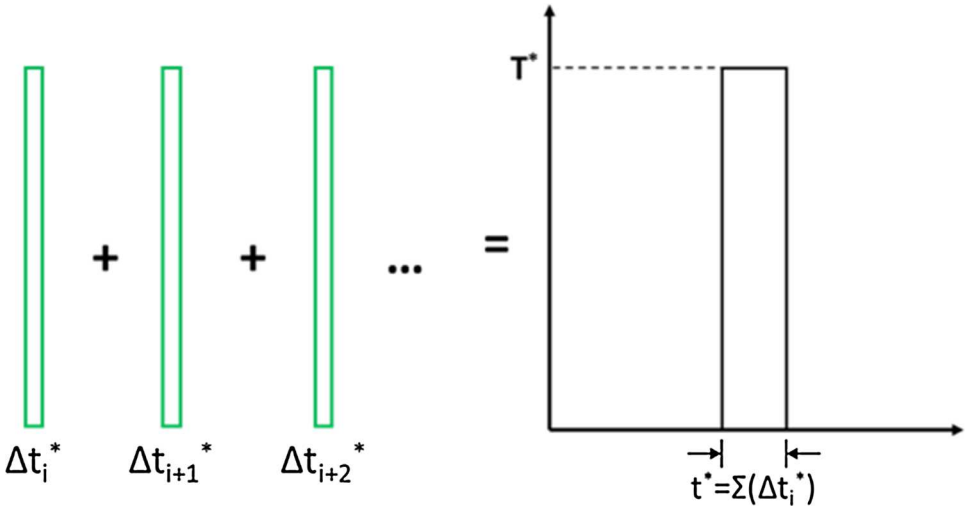

Fig. 3. Addition of Δt_i^* values to generate an equivalent isothermal cycle with temperature T* and time t*.

which, in combination with computational modeling of weld thermal histories, can be used in development and optimization of efficient temper bead welding procedures. The proposed methodology addresses the microstructural aspect of tempering, as reflected by hardness reduction, in steels that undergo martensitic and/or bainitic transformation in the HAZ during welding. Such phase transformation behavior covers a wide range of carbon-manganese, low, medium, and high alloy ferritic and martensitic steels, regularly used in oil and gas, petrochemical, fossil and nuclear power generation, and defense applications.

2. Materials and methods

2.1. Temper bead thermal history acquisition

A set of thermal histories was collected from the HAZ of Alloy 625 filler metal weld overlay (WOL) on a Grade 22 steel plate. The latter was delivered in normalized (905 °C for 41 min, air cooled) and tempered (727 °C for 67 min, air cooled) condition. The chemical compositions of the base and filler metals are shown in Table 1. The WOL contained three layers and was made using a gas tungsten arc welding – cold wire (GTAW-CW) process with parameters adapted from a temper bead procedure used in industry, Table 2. The first, second, and third layer contained correspondingly eight, seven, and four beads that were 150 mm long. The base metal plate had dimensions of 150 mm × 200 mm and was 25 mm thick. The thermal data was collected at a 500 Hz sampling rate using type K thermocouples and a fast sampling data acquisition system. The thermocouples were welded into 1.6 mm diameter holes drilled into the plate bottom side at distances between 0.3 and 1.5 mm from the expected fusion boundary location, Fig. 4. Eight thermocouples were located beneath the two central beads of the first layer, equally spaced along the longitudinal direction of the WOL. Thermal histories with maximum temperatures corresponding to the coarse-grained and inter-critical heat affected zone (CGHAZ and ICHAZ) were collected. A summary of the measured peak temperatures in all eight thermal histories collected from the three-layer weld overlay is shown in Table 3. An example of a thermal history with multiple reheats experienced in the CGHAZ 0.3 mm below the fusion boundary is shown in Fig. 5.

2.2. Controlling factors of tempering

A design of experiment (DoE) approach was used to quantify the factors controlling the HAZ tempering response during welding. The effects of heating rate, peak temperature, and cooling rate of a single tempering cycle were evaluated using Box-Behnken DoE. The DoE matrix of tempering simulations is shown in Table 4. The experiments included 15 simulations of CGHAZ microstructure followed by a single tempering cycle with peak temperature below the A_{C1} temperature.

The simulations were performed using the Gleeble® thermal-mechanical simulator on cylindrical samples with 6.4 mm diameter and 51 mm length machined from the Grade 22 plate used as WOL substrate. The tempering cycles replicated thermal histories recorded in the experimental WOL. The CGHAZ simulations reproduced the thermal history of pass number 5 recorded by thermocouple TC7 that had peak temperature of 1334 °C and cooling time between 800 and 500 °C ($t_{8/5}$) of 9 s, Table 3 and Fig. 5. A Gleeble® simulation of this thermal history resulted in a martensitic microstructure with hardness of 417 HV_1. The dilation curve in Fig. 6 was used for determination of the A_{C1}, A_{C3}, M_S, and M_F temperatures. The DoE results were applied to develop a predictive equation for the CGHAZ hardness as a function of tempering cycle peak temperature, heating rate, and cooling rate.

Table 2
Welding Parameters Used for Each Weld Pass in the WOL.

Voltage (V)	Current (A)	Wire Feed Speed mm/min (IPM)	Travel Speed mm/min (IPM)	Heat Input kJ/mm (kJ/in)	Overlap (%)
13	180	889 (35)	91 (3.6)	991 (39)	50

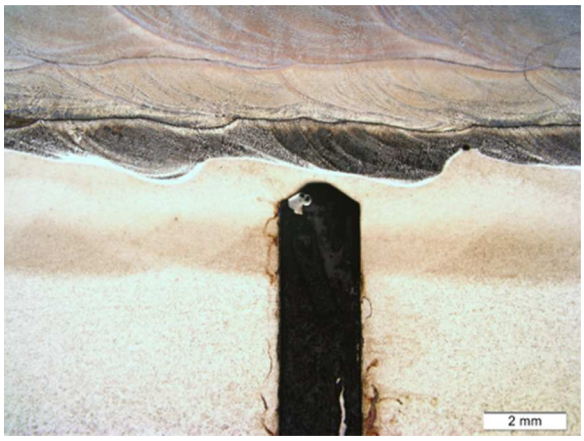

Fig. 4. Location of thermocouple in relation to WOL. Note that the WOL contained 3 layers.

2.3. Tempering response simulations

The process of bead tempering in the HAZ of multipass WOLs was recreated using the Gleeble® thermal-mechanical simulator. The simulations included 61 CGHAZ and 23 ICHAZ multiple reheat thermal histories composed from portions of the experimentally collected WOL thermal histories. These contained a single CGHAZ or ICHAZ cycle with corresponding peak temperature of 1334 °C or 861 °C, followed by one to five tempering cycles with peak temperatures below the A_{C1} temperature. An example of tempering cycles imposed on a sample with a simulated CGHAZ microstructure is shown in Fig. 7. The CGHAZ and ICHAZ tempering sequences are summarized in Tables 5 and 6, respectively.

2.4. Tempering response quantification

2.4.1. Single tempering cycle

The tempering response generated by the single reheat cycles listed in Tables 5 and 6 was quantified using the approach developed by Semiatin et al. [12] of converting non-isothermal into isothermal tempering cycles. The GBP values of all single tempering cycles were calculated using Δt_i value of 0.01 s. The results were subjected to regression analysis to develop polynomial equations for the HAZ hardness as a function of the tempering cycle peak temperature and the GBP

Table 1
Chemical Compositions for the Base Metal and Filler Metal used.

	Element (wt%)														
	Fe	C	Mn	Cr	Mo	Cu	Si	Ni	Al	Nb	Co	Ti	B	P	S
F22 Steel	Bal.	0.13	0.52	2.25	0.94	0.17	0.21	0.12	0.033	0.001	–	0.003	0.0001	0.016	0.009
Alloy 625	0.23	0.01	0.04	22.23	8.61	0.03	0.04	64.7	0.1	3.59	0.01	0.21	–	0.003	0.001

Table 3
Peak temperatures of all thermal histories collected during WOL creation. Thermal cycles used for CGHAZ (1334 °C) and ICHAZ (861 °C) are highlighted in bold.

		Peak Temp (deg C)							
	Pass	TC1	TC2	TC3	TC4	TC5	TC6	TC7	TC8
TC Distance below Fusion Boundary (mm)		0	0	0.025	0	0.13	0.3	0.15	0.58
	1	142	171	152	175	154	202	165	198
	2	211	273	217	272	217	335	235	315
	3	370	527	343	503	338	730	385	661
	4	1390	1402	1066	1393	974	1233	1365	1125
1st Layer	5	1411	1055	1449	1244	1369	995	**1334**	**873**
	6	880	438	906	517	1039	384	775	369
	7	370	262	388	289	438	246	350	242
	8	219	182	230	196	248	181	224	184
	9	211	312	245	326	256	395	289	356
	10	327	521	327	539	350	693	432	594
	11	820	937	910	1008	889	983	988	838
2nd Layer	12	1022	837	1112	945	1104	784	1053	696
	13	630	525	683	559	394	369	466	355
	14	360	411	373	455	742	186	599	183
	15	269	192	293	218	328	373	268	338
	16	230	316	248	325	249	638	277	556
	17	717	740	786	791	786	738	796	641
3rd Layer	18	728	540	774	600	802	475	708	437
	19	425	307	449	337	488	283	403	277

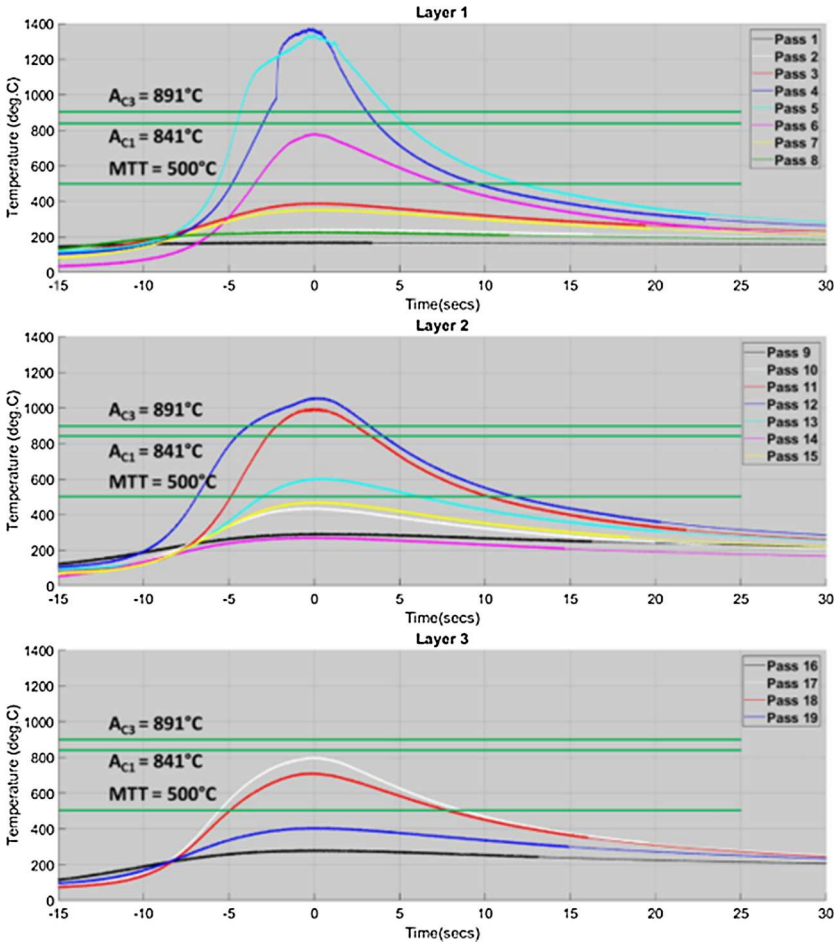

Fig. 5. Thermal history with multiple reheats in the CGHAZ recorded form a thermocouple 7 located at 0.3 mm below the fusion boundary of the weld overlay.

values.

2.4.2. *Multiple tempering cycles*

As previously discussed, a new methodology was developed for the quantification of tempering response generated by multiple tempering cycles. The methodology is based on the effective tempering parameter approach of Semiatin et al. and is demonstrated in Fig. 8. The highest peak temperature from all non-isothermal cycles is used as the equivalent tempering temperature T*. Similarly, as a single non-isothermal cycle, the multiple non-isothermal cycles are divided into small Δt_i segments. The corresponding equivalent Δt_i^* segments are calculated using the T* value and Eq.s (5)–(7). The T* and $\sum \Delta t_i^*$ values

Table 4
DoE Test Matrix of CGHAZ Single Tempering Cycle Response.

Sample	Heating Rate (°C/s)	Cooling Rate (°C/s)	Peak Temperature (°C)	Predicted Hardness (HV)	Measured Hardness (HV)
1	50	70	500	379	389
2	20	40	500	410	401
3	80	40	500	414	408
4	80	70	643	404	399
5	80	40	785	332	334
6	20	70	643	385	382
7	50	40	643	382	377
8	50	70	785	347	336
9	50	10	500	399	404
10	50	40	643	375	377
11	20	10	643	386	388
12	50	40	643	378	377
13	50	10	785	330	312
14	80	10	643	384	383
15	20	40	785	330	329

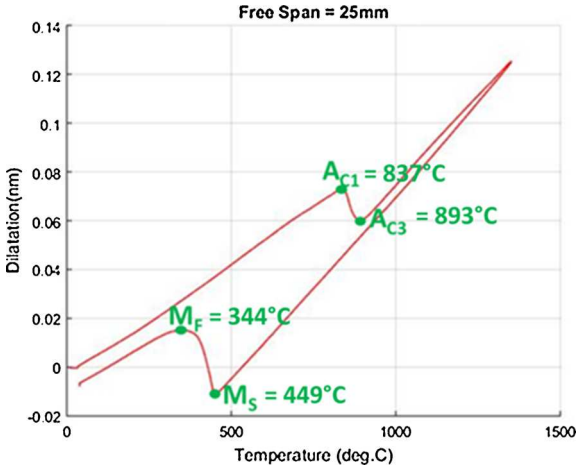

Fig. 6. Dilation curve of phase transformation in CGHAZ of grade 22 steel. Gleeble™ simulation of an experimentally recorded weld overlay thermal history with a peak temperature of 1334 °C, a $t_{8/5}$ time of 9.0 s, and hardness of 413HV_1.

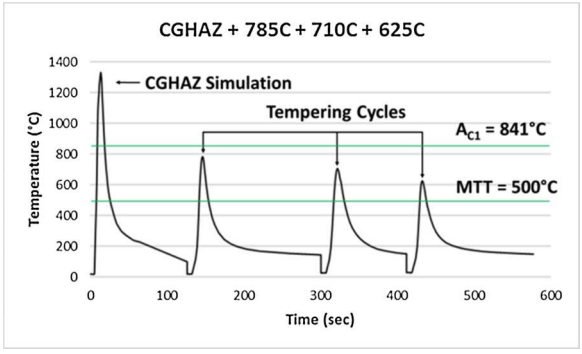

Fig. 7. Example of a Gleeble™ simulated CGHAZ with three tempering cycles.

determined with this procedure are used for calculation of a GBP parameter value that accounts for the tempering effect of multiple thermal cycles. The results from the multiple reheat simulations were subjected to regression analysis to develop polynomial equations for the HAZ hardness as a function of the calculated GBP values.

2.5. Metallurgical characterization

All tempering response simulation samples were cross-sectioned next to the thermocouple location, mounted, polished, and etched using conventional metallography techniques. The hardness was determined as an average value of ten Vickers indents performed with 1 kg load. Metallurgical characterization was performed using light optical microscopy. The weld overlay was cross sectioned at thermocouple 6, located in the CGHAZ, and subjected to hardness mapping with automatic Vickers hardness tester at 1 kg load and 250 μm step. Carbon replica films were generated from both a base metal and CGHAZ +785 °C (x5) sample to extract the carbides present. The carbon replicas were then imaged in the TEM. In addition, energy dispersive X-ray spectroscopy was performed on these carbon replica films to map the chemical compositions of typical carbides present in each sample.

3. Results

3.1. Weld overlay thermal history acquisition

The results of the HAZ thermal history acquisitions are summarized in Table 3. The thermal histories recorded by thermocouple 7 are shown in Fig. 5. All thermocouples remained connected throughout the overlay deposition and measured the HAZ thermal histories generated by each of the three layers. The first layer peak temperatures recorded by thermocouples 1 through 4 may be inaccurate, since the thermocouples were potentially exposed to liquid metal at the fusion boundary.

3.2. Controlling factors of tempering

The hardness testing results from the DoE study are summarized in Table 4. The separate and combined effects of the thermal history peak temperatures, heating and cooling rates on the tempering response in the simulated CGHAZ are shown in Table 7. Based on the DoE study, a predictive equation for the CGHAZ hardness resulting from a single weld tempering cycle was developed, Eq. (8).

$$\begin{aligned} CGHAZ\ Hardness\ (HV) = {} & 376.67 - 36.4{*}PT - 18.3{*}PT^2 + 9.7{*}(CR{*}PT) \\ & + 9.6{*}\ HR^2 + 5.25{*}(HR{*}CR) + 2.8{*}HR \\ & + 2.5{*}CR + 1.8{*}CR^2 - 0.5{*}(HR{*}PT) \end{aligned} \quad (8)$$

where PT is the tempering cycle peak temperature, CR is the cooling rate, and HR is the heating rate. This predictive equation provided a very good correlation, with R^2 value of 0.95, to the experimental results, Fig. 9. As shown in Table 5, the cooling rate, the heating rate, and their interactions with the peak temperature have probability terms (t) larger than 0.05. Therefore, the heating and cooling rates of the tempering reheat cycles have insignificant effect on the HAZ hardness within the DoE ranges of variation defined in Table 4.

3.3. Tempering response quantification

The tempering response results from the single and multiple reheat CGHAZ and ICHAZ simulations are summarized in Tables 5 and 6. As shown in Table 5, single tempering cycles with peak temperature below 500 °C did not provide appreciable tempering effects in terms of hardness reduction. Therefore, 500 °C was selected as the minimum tempering temperature (MTT) for the further tempering simulations of the HAZ in the tested heat of Grade 22 steel.

A plot of the resulting hardness values vs. the peak temperatures of single tempering cycles is shown in Fig. 10, for both CGHAZ and ICHAZ microstructures. The resulting regression equations provide hardness prediction with good correlation to the peak temperatures of single tempering cycles, R^2 of 0.90 for the CGHAZ (Eq. (9)) and R^2 of 0.82 for

Table 5
Tempering response simulations in CGHAZ of Grade 22 steel. Tempering cycle's maximum temperature (°C) and sequences 1 to 5 and resulting hardness and GBP values.

CGHAZ															
Tempering Cycle								Tempering Cycle							
1	2	3	4	5	Replicates	Hardness (HV)	GBP	1	2	3	4	5	Replicates	Hardness (HV)	GBP
–	–	–	–	–	2	413, 413	–	738	738	–	–	–	2	313, 307	27585
500	–	–	–	–	2	399, 410	20225	785	785	–	–	–	2	297, 309	28924
505	–	–	–	–	1	404	20790	500	500	500	–	–	2	381, 391	20886
540	–	–	–	–	1	387	21940	600	600	700	–	–	1	341	25639
550	–	–	–	–	1	395	21545	600	700	600	–	–	1	355	25639
595	–	–	–	–	1	389	23380	600	700	700	–	–	1	351	26122
600	–	–	–	–	1	380	22873	600	785	785	–	–	1	290	28925
625	–	–	–	–	1	377	24199	700	785	785	–	–	1	290	28943
643	–	–	–	–	2	371, 370	24019	643	643	643	–	–	2	365, 377	24806
650	–	–	–	–	1	374	24252	690	690	690	–	–	2	340, 329	26739
660	–	–	–	–	1	385	24858	738	738	738	–	–	2	308, 298	27905
690	–	–	–	–	2	335, 333	25913	785	785	785	–	–	2	289, 302	29259
700	–	–	–	–	1	366	25582	500	500	500	500	–	2	377, 380	21059
710	–	–	–	–	1	347	26451	643	643	643	643	–	2	372, 373	25012
738	–	–	–	–	2	318, 318	27037	690	690	690	690	–	2	338, 351	26955
741	–	–	–	–	1	326	27234	738	738	738	738	–	2	307, 301	28132
750	–	–	–	–	1	322	26932	785	785	785	785	–	2	277, 303	29497
500	500	–	–	–	2	393, 383	20642	500	500	500	500	500	2	379, 387	21193
600	700	–	–	–	2	339, 351	25611	643	643	643	643	643	2	359, 376	25172
643	643	–	–	–	2	362, 365	24516	690	690	690	690	690	2	322, 335	27123
690	690	–	–	–	2	336, 333	26434	785	785	785	785	785	2	291, 290	29681

Table 6
Tempering response simulations in ICHAZ of Grade 22 steel. Tempering cycle's maximum temperatures (°C) and sequences 1 to 5 and resulting hardness and GBP values.

ICHAZ															
Tempering Cycle								Tempering Cycle							
1	2	3	4	5	Replicates	Hardness (HV)	GBP	1	2	3	4	5	Replicates	Hardness (HV)	GBP
–	–	–	–	–	2	286, 294	–	643	643	–	–	–	1	280	24516
500	–	–	–	–	2	293, 286	20225	600	700	–	–	–	1	262	25611
505	–	–	–	–	1	297	20790	690	690	–	–	–	1	260	26434
540	–	–	–	–	1	290	21940	738	738	–	–	–	1	230	27585
550	–	–	–	–	1	286	21545	785	785	–	–	–	2	247, 254	28924
595	–	–	–	–	1	263	23380	500	500	500	–	–	2	263, 283	20886
600	–	–	–	–	2	271, 288	22873	600	700	600	–	–	1	264	25639
625	–	–	–	–	1	262	24199	643	643	643	–	–	1	284	24806
650	–	–	–	–	1	261	24252	690	690	690	–	–	1	262	26739
660	–	–	–	–	1	261	24858	738	738	738	–	–	1	239	27905
700	–	–	–	–	1	259	25582	785	785	785	–	–	2	221, 227	29259
710	–	–	–	–	1	239	26451	500	500	500	500	–	2	276, 278	21059
741	–	–	–	–	1	240	27234	643	643	643	643	–	1	280	25012
750	–	–	–	–	1	229	26932	785	785	785	785	–	2	217, 199	29497
785	–	–	–	–	2	251, 255	28351	500	500	500	500	500	2	282, 271	21193
500	500	–	–	–	2	296, 298	20642	785	785	785	785	785	2	213, 204	29681

the ICHAZ (Eq. (10)).

$$CGHAZ\ Hardness\ (HV) = -0.0007{*}PT^2 + 0.5871{*}PT + 291.02 \quad (9)$$

$$ICHAZ\ Hardness\ (HV) = 0.0003{*}PT^2 - 0.609{*}PT + 518.42 \quad (10)$$

A plot of the hardness values resulting from single reheat tempering cycles vs. the corresponding GBP values is shown in Fig. 11, for both CGHAZ and ICHAZ microstructures. The resulting regression equations provide hardness prediction with good correlation to the GBP values of single tempering cycles, R^2 of 0.91 for the CGHAZ (Eq. (11)) and R^2 of 0.84 for the ICHAZ (Eq. (12)).

$$CGHAZ\ Hardness\ (HV) = -9x10^{-7}{*}GBP^2 + 0.032{*}GBP + 130.32 \quad (11)$$

$$ICHAZ\ Hardness\ (HV) = 6x10^{-7}{*}GBP^2 - 0.0374{*}GBP + 792.78 \quad (12)$$

The GBP values of the multiple reheat experiments in Tables 5 and 6 were calculated with the newly developed methodology demonstrated in Fig. 8. The measured hardness values resulting from multiple reheat cycles are plotted vs. the corresponding GBP values in Fig. 12. The resulting regression equations provide hardness prediction with good correlation to the GBP values of multiple tempering cycles, R^2 of 0.90 for the CGHAZ (Eq. (13)) and R^2 of 0.82 for the ICHAZ (Eq. (14)).

$$CGHAZ\ Hardness\ (HV) = -1x10^{-6}{*}GBP^2 + 0.04{*}GBP + 11.216 \quad (13)$$

$$ICHAZ\ Hardness\ (HV) = -6x10^{-7}{*}GBP^2 + 0.0243{*}GBP + 53.335 \quad (14)$$

The proposed polynomial equations were developed by fitting experimental data for GBP values between 20,225 and 29,700 (Tables 5 and 6), which defines their application range. At the lower end of GBP 20225, which reflects no tempering at short reheats to or below the MTT (500 °C), the polynomial equations reproduce the original CGHAZ and ICHAZ hardness values, Tables 5 and 6. The application range of these equations covers the typical spectrum of thermal histories experienced in the HAZ of cold wire GTAW weld overlays.

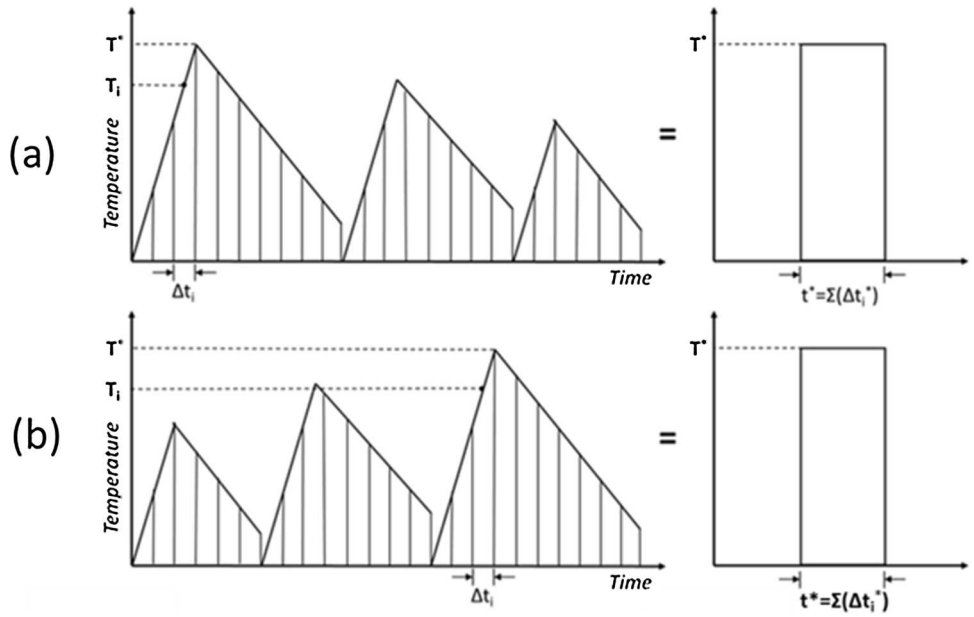

Fig. 8. Extension of the modified Grange-Baughman Parameter technique to apply to multiple tempering cycles, including those with (a) descending peak temperatures and (b) ascending peak temperatures.

Table 7
Sorted Parameter Estimates for Terms from Design of Experiment.

Sorted Paramater Estimates					
Term	Estimate	Std Error	t Ratio		Prob> |t|
Peak Temp (500, 800)	-36.43709	4.003803	-9.1		0.0003*
Peak Temp*Peak Temp	-18.31825	6.128348	-2.99		0.0305*
Cooling Rate*Peak Temp	9.746939	5.593428	1.74		0.1419
Heating Rate*Heating Rate	9.5833	5.593428	1.73		0.1437
Heating Rate*Cooling Rate	5.25	5.313773	0.99		0.3685
Heating Rate (20, 80)	2.849807	3.767118	0.76		0.4835
Cooling Rate (10, 70)	2.471102	3.767118	0.66		0.5408
Cooling Rate*Cooling Rate	1.8333	5.53075	0.33		0.7537
Heating Rate*Peak Temp	-0.521234	5.593428	-0.09		0.9294

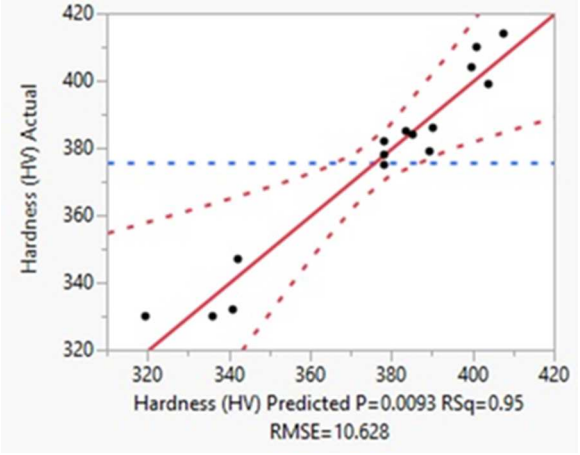

Fig. 9. Regression plot developed using Design of Experiment studying the effects of heating rate, cooling rate, and peak temperature of a tempering cycle on hardness.

3.4. Experimental validation

The hardness prediction Eq. (12) developed for multiple CGHAZ reheats was applied to two thermocouple locations from the weld overlay and compared to hardness values at those locations. The two thermocouples (TC6 and TC8) were located in the CGHAZ of the weld overlay and experienced several reheats above the A_{C3} temperature followed by several tempering reheats below the A_{C1} temperature, as shown in Figs. 13 and 14. The hardness maps generated in the vicinity of the thermocouple holes are shown in Figs. 15 and 16. Table 8 lists the GBP values that were used in the hardness predictions and compares the hardness values predicted with Eq. (14) to the average of hardness of seven indents located next to the thermocouple tip.

3.5. Metallurgical characterization

Fig. 17 demonstrates the effect of the tempering cycle peak temperature and of multiple reheats on the resulting microstructure and HAZ hardness. Fig. 18 presents TEM images of the carbide distribution and density, and typical carbide morphologies in Grade 22 base metal and simulated CHGAZ subjected to multiple weld tempering cycles. EDS compositional maps in representative carbides from these two conditions are shown in Fig. 19 through 22 .

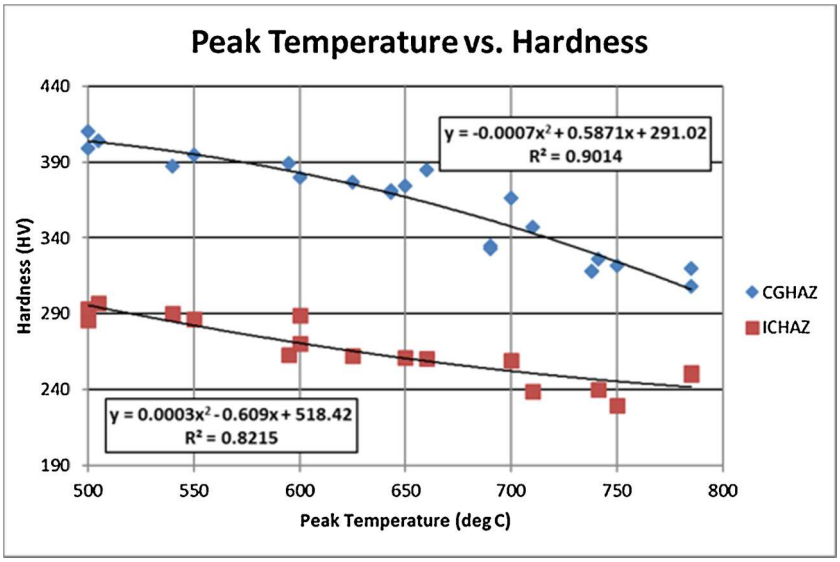

Fig. 10. Hardness (y) vs. peak temperature (x) of tempering cycle for all CGHAZ and ICHAZ samples undergoing a single reheat tempering cycle.

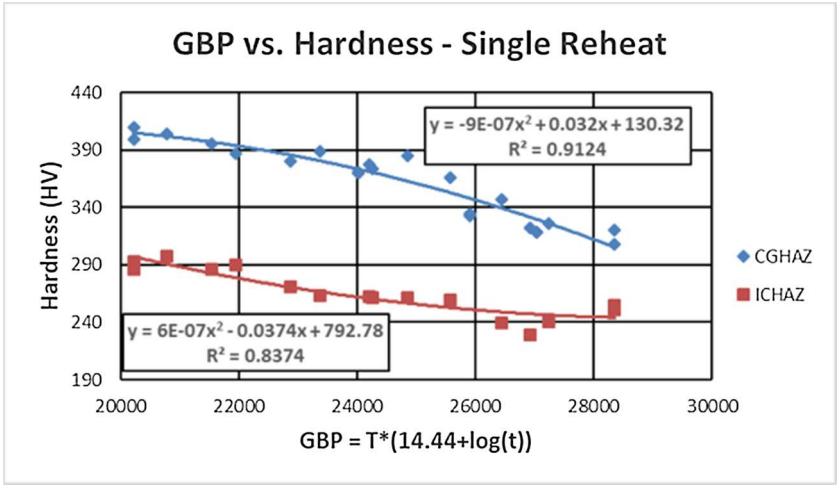

Fig. 11. Hardness (y) vs. GBP (x) for CGHAZ and ICHAZ samples experiencing a single reheat tempering cycle.

4. Discussion

4.1. Methodology for tempering response quantification in temper bead welding

Past work on quantification of the tempering response during heat treatment has mostly been limited to isothermal conditions, Hollomon and Jaffe [7] Grange and Baughman [10]. The Hollomon-Jaffe and Grange-Baughman parameters utilize empirical relationships that describe tempering as a thermally-activated process, where the interaction of time and temperature follows a diffusion type relationship. There have been some studies on quantifying the tempering response during non-isothermal heat treatments, Semiatin [12], but nearly all these addressed only a single tempering thermal cycle. The neural network approach developed by Yu et al. [14] has successfully predicted hardness in samples experiencing multiple non-isothermal cycles. However, this approach requires separate "training" of the neural network for each alloy and involves a large number of physical simulation experiments. Yu et al. [15] applied the TCTP parameter for quantification of the effect of conventional PWHT, including the effects of heating and cooling rates, on hardness reduction. This parameter is inapplicable for temperbead welding, which involves 3–4 orders of magnitude faster heating and cooling rates.

The proposed methodology for quantification of tempering response from multiple non-isothermal tempering cycles utilizes a modification of the Grange Baughman Parameter and therefore reflects the tempering phenomenon as a thermally-activated process. The methodology involves the following steps:

- Experimental determination of the A_{C1}, A_{C3}, and MTT on samples of the tested steel, using typical temper bead weld thermal cycles
- Physical simulations of a GCHAZ and ICHAZ microstructures followed by up to five tempering cycles with peak temperatures between the A_{C1} and MTT
- Hardness measurements on all tested samples
- GBP value calculation for each tempering simulation using a newly developed procedure that accounts for the effect of multiple tempering reheats
- Generation of hardness versus GBP polynomial equations for the tempering response in CGHAZ and ICHAZ, using regression analysis of the experimental results.

Based on the results of this study, about 40 tempering simulations are needed to produce tempering response equations that are well

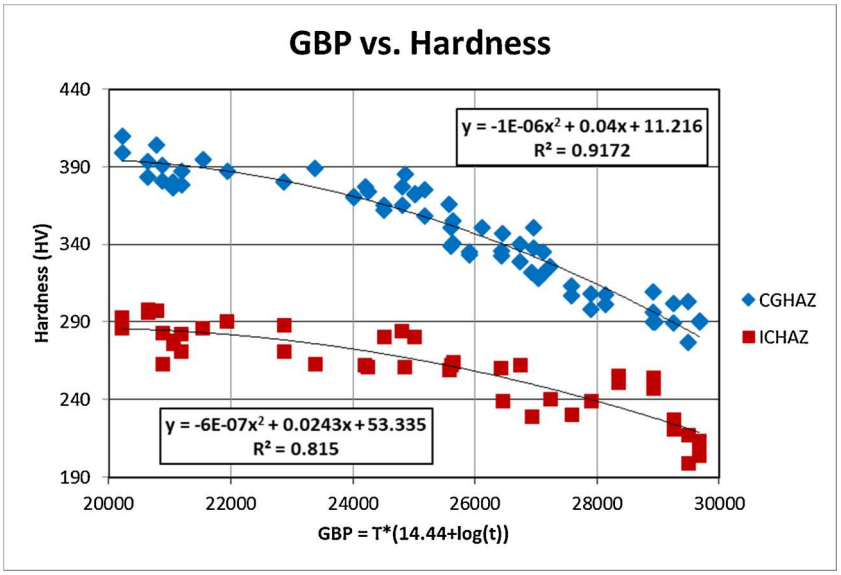

Fig. 12. Measured hardness (y) in all CGHAZ and ICHAZ samples vs. Grange-Baughman Parameter values (x) calculated using the proposed methodology for multiple tempering cycles.

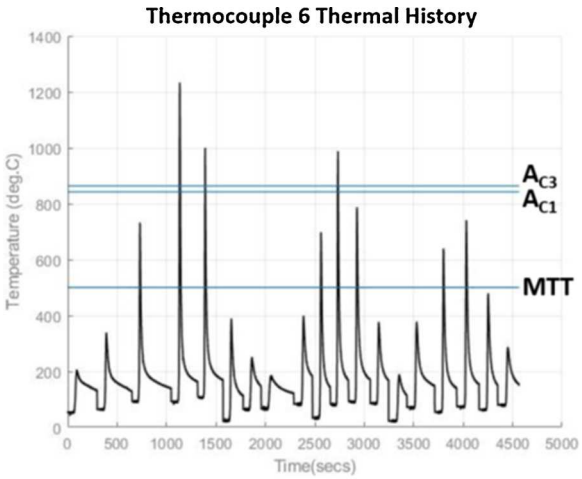

Fig. 13. Thermal history for thermocouple 6 located 0.30 mm below the fusion boundary. Note: the rapid cooling in the range of 150 °C to 100 °C is related to record interruption in between the weld beads.

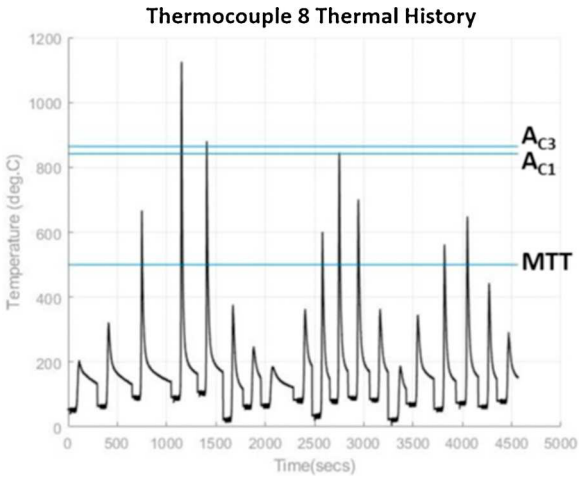

Fig. 14. Thermal history for thermocouple 8 located 0.58 mm below the fusion boundary.

correlated. The proposed methodology for quantification of tempering response from multiple tempering cycles was applied to calculate the GBP values of the experimental thermal histories summarized in Tables 5 and 6. The plots of the measured CGHAZ and ICHAZ hardness versus the calculated GBP values (Fig. 12) and the resulting polynomial equations (Eqs. (13) and (14)) demonstrated a very good correlation with R^2 values of 0.92 and 0.82. For comparison, Yu et al. [15] reported R^2 values of 0.95 for the TCTP parameter they developed for ASME SA350 Gr.LF5 steel.

The proposed methodology was validated by comparing the measured hardness at TC locations 6 and 8 to the hardness predictions of Eq. (12). The measured hardness represents an average value of the seven hardness indents closest to the TC tip locations in the hardness maps in Figs. 15 and 16. The predicted hardness was calculated with GBP values determined using the thermal histories recorded by TCs 6 and 8, which are shown in Figs. 13 and 14. The results in Table 8 show very good correlation between the predicted hardness and measured average hardness value next to the thermocouple tip. The predicted hardness values for TC6 and TC 8 were correspondingly 2.04 % and 1.25 % lower than the measured ones.

The location of TC6 experienced three thermal cycles above the A_{C3} temperature, two in the first WOL layer and one in the second layer, that would erase previous tempering effects and generate fresh martensite. These were followed by three tempering cycles between the MTT and A_{C1} temperatures, one in the second WOL layer and two in the third layer. The location of TC8 experienced two thermal cycles above the A_{C3} temperature in the first layer followed by five tempering cycles between the MTT and A_{C1} temperatures: three in the second layer and two in the third layer. Due to the larger number of tempering cycles, this location had lower measured hardness and predicted GBP and hardness values than the location of TC6, Table 8.

4.2. *Controlling factors of tempering*

The results of the performed DoE study show that, in case of single short term tempering cycles, the peak temperature of the tempering cycle is the best indicator of the resulting hardness. This is evident from the information in Tables 4 and 7. The heating and cooling rates were determined as insignificant factors within their corresponding limits of

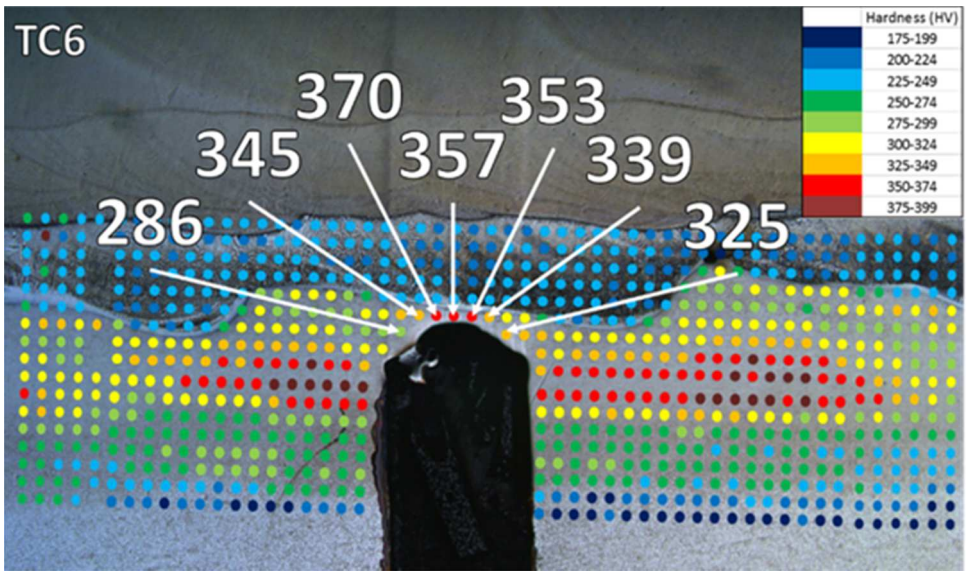

Fig. 15. Hardness indents around thermocouple 6 from the weld overlay.

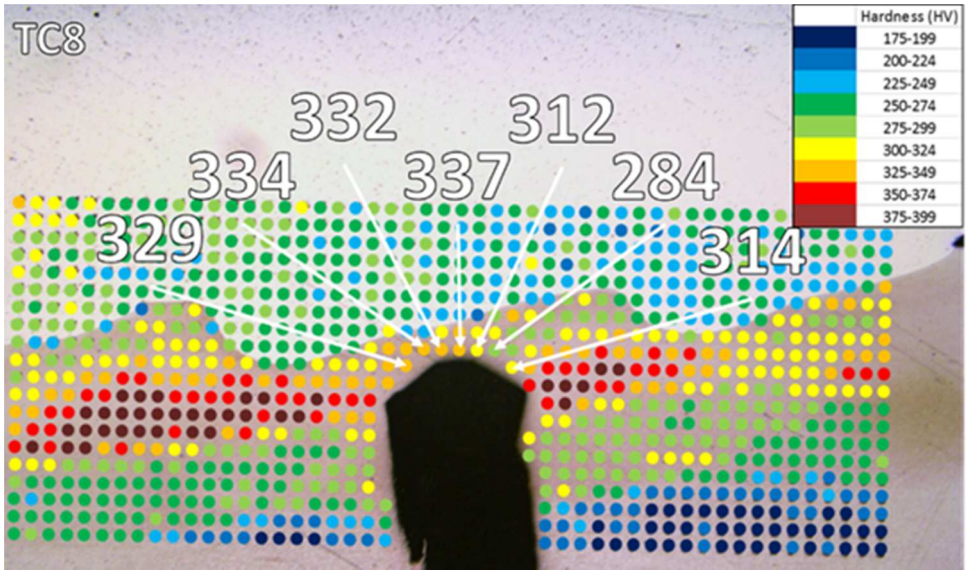

Fig. 16. Hardness indents around thermocouple 8 from the weld overlay.

Table 8
Summary of hardness prediction validation for thermocouples 6 and 8 from the weld overlay.

Thermocouple	Microstructure	GBP Value	Estimated Hardness	Experimental Hardness	Deviation, %
6	CGHAZ	28630	324	332	2.04
8	CGHAZ	29100	316	320	1.25

variation. The latter are shown in Table 4 and reflected the heating and cooling rates measured in the experimental WOL, which can be considered typical for a wide range of arc welding applications. The polynomial equation developed form the DoE study (Eq. (7)) has acceptable accuracy that is demonstrated by comparison of predicted and measured hardness values in Table 4 and by the R^2 value in Fig. 9.

The series of single reheat tempering experiments listed in Tables 5 and 6 provided additional validation of the DOE study results. The GBP values for these experiments were calculated using the approach of Semiatin et al. [12] that accounts for the effect of the heating and cooling rates. The CGHAZ hardness prediction formulae based on the tempering cycle peak temperature (Eq. (9)) and on the calculated GBP value (Eq. (11)) had close R^2 values, correspondingly of 0.90 and 0.91. The ICHAZ hardness prediction formulae (Eqs. (10) and (12)) also had close R^2 values of 0.82 and 0.84, as shown in Figs. 10 and 11. These results confirmed that the heating and cooling rates had insignificant effect on the tempering response generated by single short term reheats.

Eqs. (8) through (12) can be used for estimating the hardness reduction effect from single tempering cycles in the HAZ of the studied heat of Grade 22 steel. The knowledge that the peak temperature of a short-term tempering cycle is the most significant factor controlling HAZ hardness is useful when considering instances of single tempering

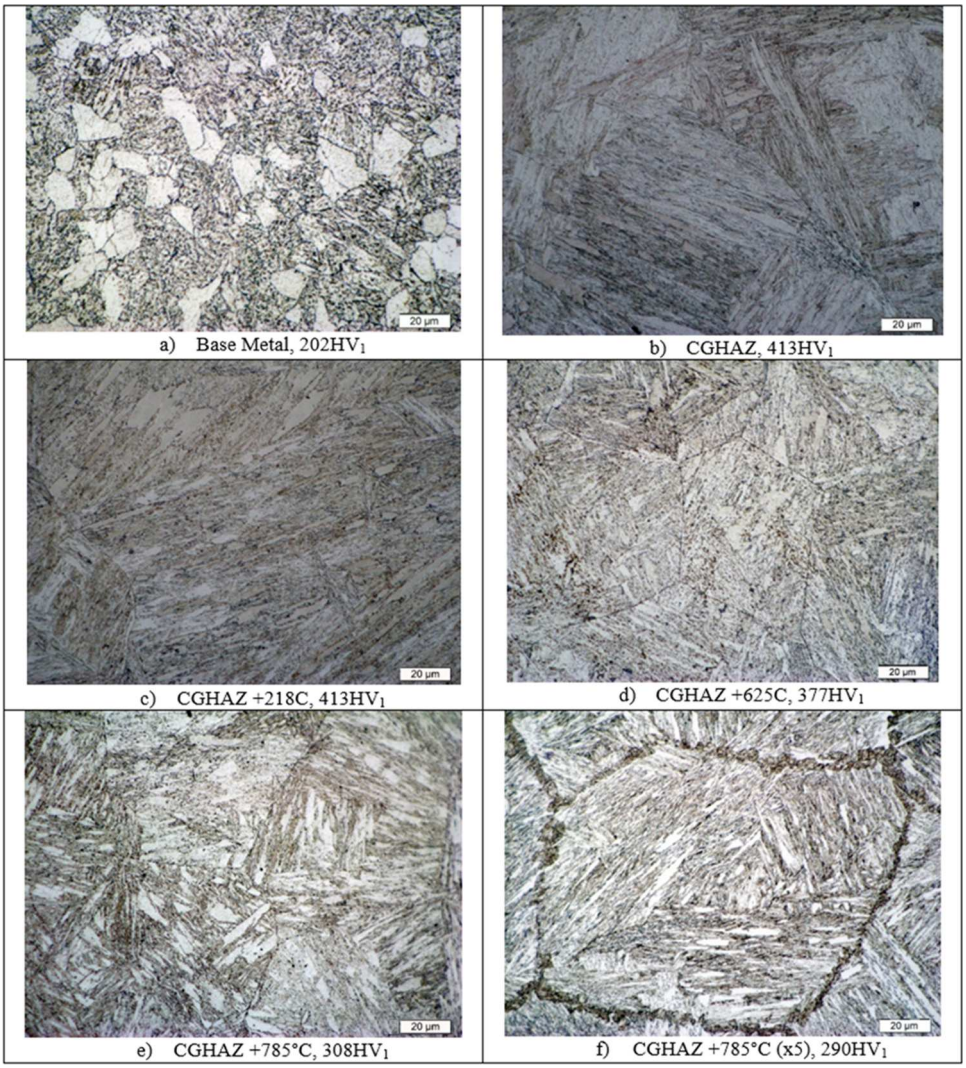

Fig. 17. Effect of tempering reheats on the HAZ hardness and microstructure in Grade 22 steel.

reheats, i.e. the effect of the last bead in a single layer weld overlay, or the last bead in a multipass weld.

4.3. Weld overlay tempering efficiency

The values and sequences of peak temperatures experienced at the thermocouple locations, shown in Table 3, were analyzed to evaluate their effect on the tempering efficiency of the experimental WOL. The analysis was based on the assumption that a peak temperature exceeding the A_{C1} or A_{C3} would generate fresh martensite in the HAZ, erasing the tempering effect of previous reheats between the MTT and A_{C1} temperatures.

Based on the above assumption, the tempering effect of each WOL layer was summarized in Table 9. Only thermocouple locations TC4 and TC7 experienced a tempering reheat between the MTT and the A_{C1} temperature in the first layer, which was erased by reheats above the A_{C3} in the second layer. TC 8, located 0.58 mm below the fusion boundary, experienced three tempering cycles in the second layer and two in the third layer. The thermocouple locations closer to the fusion boundary experienced one tempering cycle in the second layer and two in the third layer.

The hardness at all thermocouple locations was predicted using the proposed approach for quantification of tempering generated by multiple reheats. The predicted hardness reduction of 15.7%–26.9%, or up to 110 HV_1 form the original HAZ hardness of 413 HV_1, shown in Table 9, confirms that the WOL procedure applied in this study generates a significant level of tempering in the CGHAZ of the Grade 22 steel substrate. However, areas of HAZ located further from the fusion boundary experienced lower degree of tempering as can be seen in the hardness maps in Figs. 15 and 16. This could be related to smaller number and/or lower peak temperatures of tempering reheats affected by the thickness of the first and second WOL layers. Therefore, tempering efficiency evaluation of WOL procedures would require comprehensive information for the thermal histories experienced throughout the HAZ. Such information can be generated by computational modeling. Thermocouple measurements of HAZ thermal histories can be used for calibration and validation of modeling predictions, as well as for validation of the proposed approach for quantification of tempering by multiple reheats.

The physical simulation results in Tables 5 and 6 can be used to evaluate the effect of single and multiple short-term tempering reheats on the resulting CG and ICHAZ hardness. The level of hardness reduction increases with increasing the tempering cycle peak temperature and the number of tempering reheats. The single tempering cycles with peak temperatures just below the A_{C1} have the strongest tempering effect, reducing the original CG and ICHAZ hardness with up to 100 HV and 40 HV, correspondingly. The tempering efficiency of subsequent tempering reheats gradually decreases with the number of reheats. Adding up to five reheats at 785 °C further reduces the CG and ICHAZ hardness correspondingly with about 25 HV and 45 HV.

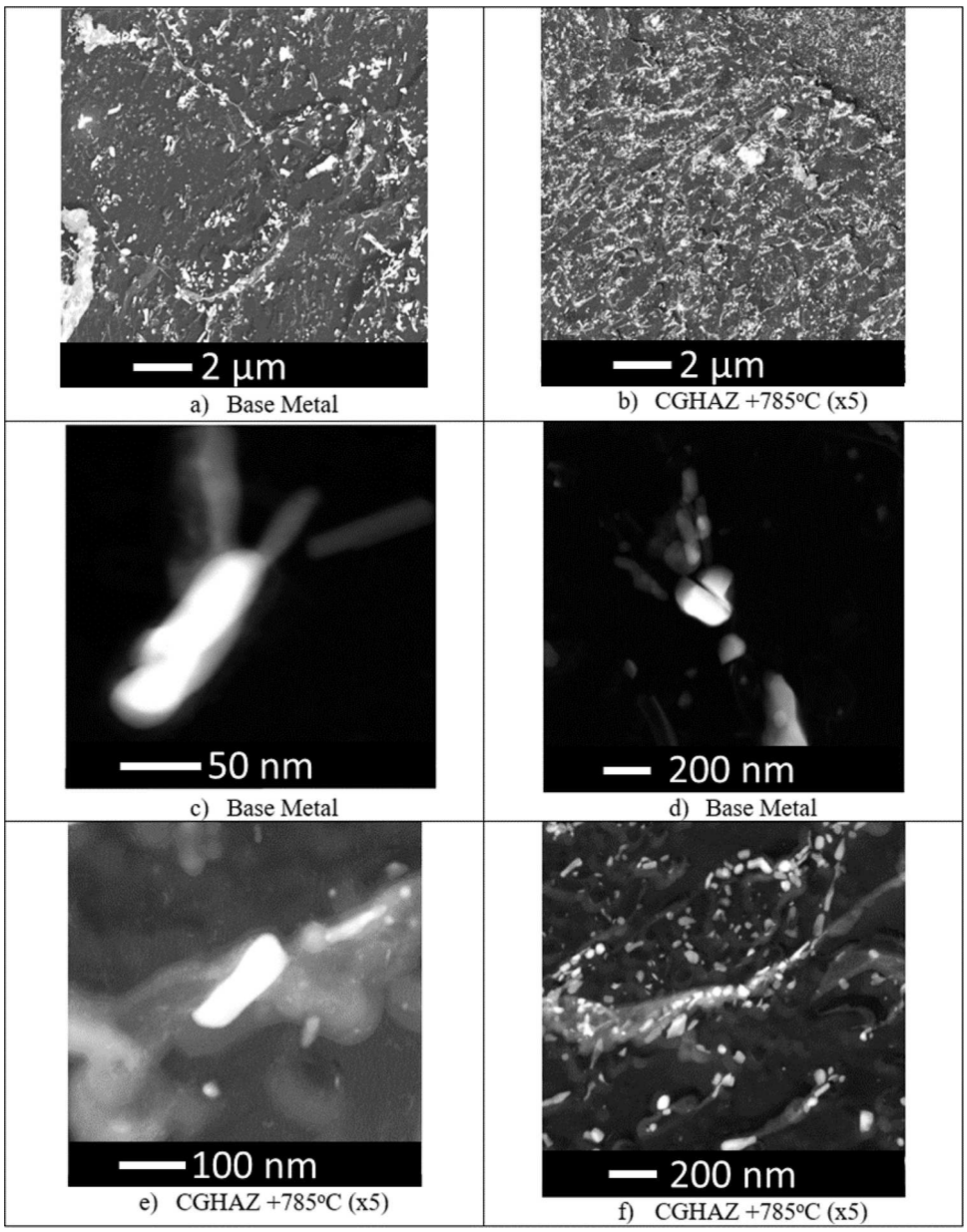

Fig. 18. TEM images of carbides in Grade 22 steel normalized and tempered base metal and simulated CGHAZ subjected to multiple weld tempering cycles.

The results of this study are of practical significance in terms of development and optimization of temper bead welding procedures. High temperature reheats below the A_{C1} generated from weld bead overlaps in the first layer and/or from weld beads in the second layer would be most efficient in hardness reduction.

4.4. *Effect of temper bead welding on HAZ microstructure and hardness*

The long exposure to high temperatures during conventional heat treatments provides conditions for a growth-controlled precipitation mechanism, driven by longer diffusion distances of carbon and alloying elements. The Grade 22 steel base metal used in this study was subjected to normalization and tempering heat treatment, which resulted in a hardness of $202HV_1$ and a microstructure with a lower density of coarse carbides preferentially precipitated at grain and microconstituent boundaries, Fig. 18a. Examples of such carbides with rod-like and globular morphologies and size in the range of 200 nm, as well as chemistries rich in Fe, Cr, Mo, and Mn with traces of Ni, are shown in Figs. 18c,d, 19, and 20 . For similar heat treatment conditions of Grade 22 steel, Dépinoy et al. [5] identified rod-like $M_{23}C_6$ carbides as well as trapezoidal and globular M_7C_3 carbides containing Fe, Cr, and Mo. Tempering at 725 °C for 5.5 h resulted in full dissolution of M_3C, partial dissolution of M_7C_3 and M_2C, and in precipitation of $M_{23}C_6$. The observed softening was related to precipitation and coarsening of $M_{23}C_6$.

Subjected to CGHAZ simulation, the normalized and tempered base metal, Fig. 17a, transformed to an almost fully martensitic microstructure with some bainitic constituent, mostly located at the prior austenite grain boundary (PAGB) triple points, Fig. 17b. The time-temperature diagram of carbide stability in steels HAZ proposed by Easterling [20] shows that the carbides present in the Grade 22 steel base metal would completely dissolve in the CGHAZ during welding. Low temperature reheats below the MTT do not change the original CGHAZ microstructure and hardness, Fig. 17c. Single reheats between the MTT and A_{C1} result in carbide precipitation within the original martensitic and bainitic constituents, with increased density of carbide population and reduction in hardness associated with higher weld cycle peak temperatures, Fig. 17d and e.

Multiple subsequent reheats just below the A_{C1} temperature had

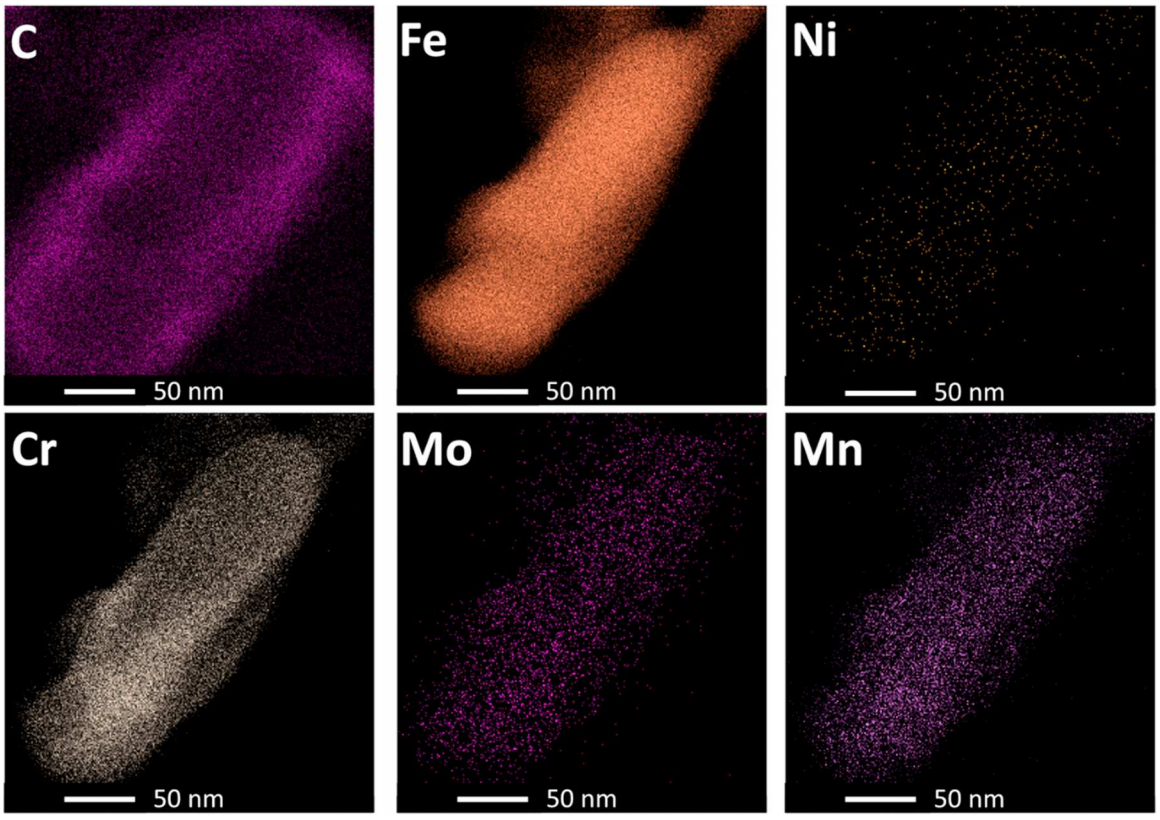

Fig. 19. EDS compositional maps in the rod-like base metal carbide 22 shown in Fig. 19c.

Table 9
Peak temperatures and predicted tempering efficiency at the experimental WOL thermocouple locations.

TC	Distance from FB (mm)	Layer 1			Layer 2			Layer 3			Effective Tempering Cycles	GBP	Predicted Hardness (HV)	Hardness Reduction %
		>A_{C3}	A_{C1}-A_{C3}	MTT-A_{C1}	>A_{C3}	A_{C1}-A_{C3}	MTT-A_{C1}	>A_{C3}	A_{C1}-A_{C3}	MTT-A_{C1}				
1	0	2	1	0	1	0	1	0	0	2	3	27183	348	15.74
2	0	2	0	0	1	0	1	0	0	2	3	29793	302	26.88
3	0.03	3	0	0	2	0	1	0	0	2	3	28891	320	22.52
4	0	2	0	1	2	0	1	0	0	2	3	28619	324	21.55
5	0.13	2	0	0	1	0	1	0	0	2	3	29362	311	24.70
6	0.3	2	0	0	1	0	2	0	0	1	3	28630	324	21.55
7	0.15	2	0	1	2	0	1	0	0	2	3	28893	319	22.76
8	0.58	1	1	0	0	0	3	0	0	2	5	29100	316	23.49

smaller contribution towards the overall hardness reduction, Fig. 17e and f. The tempered microstructure contains a high density of finely dispersed carbides, 18b. Examples of rod-like and globular morphology carbides containing mostly Fe and Cr, and only small traces of Mo, Mn, and Ni are shown in Figs. 18e,f, 21 , and 22 . The rod-like carbides are in the 100 nm size range, while the size of globular carbides varies in the 50–100 nm range. The multiple reheats resulted in formation of continuous chains of high-density fine carbides along the PAGBs, Figs. 17f and 18 f. Such PAGBs carbide chains are frequently observed in the CGHAZ of multipass welds in low alloy steels. The precipitation behavior during temper bead welding can be explained with the short exposure times to high temperatures, resulting in shorter diffusion distances. In accordance with Easterling and Porter [2], such precipitation behavior would be controlled by heterogeneous nucleation at dislocations, lath boundaries, and PAGBs.

The results of this study show that the HAZ softening in temperbead welding is controlled by the reheat with the maximum temperature between the MTT and A_{C1} temperatures, Tables 5 and 6, Figs. 10, and 17. The sequence of peak temperatures and the number of reheats with peak temperature just above MTT have insignificant effect on the level of hardness reduction. Multiple reheats with peak temperature just below A_{C1} provide smaller contribution to the overall hardness reduction.

In contrast with conventional tempering heat treatments, the mechanism of softening introduced by temperbead welding has not been fully clarified yet and needs further investigation. The tempering response in temperbead welding could be related to the kinetics of two overlapping phenomena: precipitation of finely dispersed carbides, observed in this study, and recovery of the dislocation structure in martensite. Hou et al. [21] demonstrated rapid decrease of dislocation density in fully martensitic microstructure of two Fe-0.15C-(1.0-4.0) Cr wt.% alloys when exposed to 5 s tempering at 700 °C. Longer exposures at this temperature did not significantly contribute to reduction in dislocation density.

The results of this study demonstrate that the tempering phenomenon in temperbead welding, as reflected by hardness reduction and precipitation behavior, is a thermally-activated process controlled by short term exposures between the MTT and A_{C1} temperatures. The strong correlation between the modified Grange-Baughman parameter,

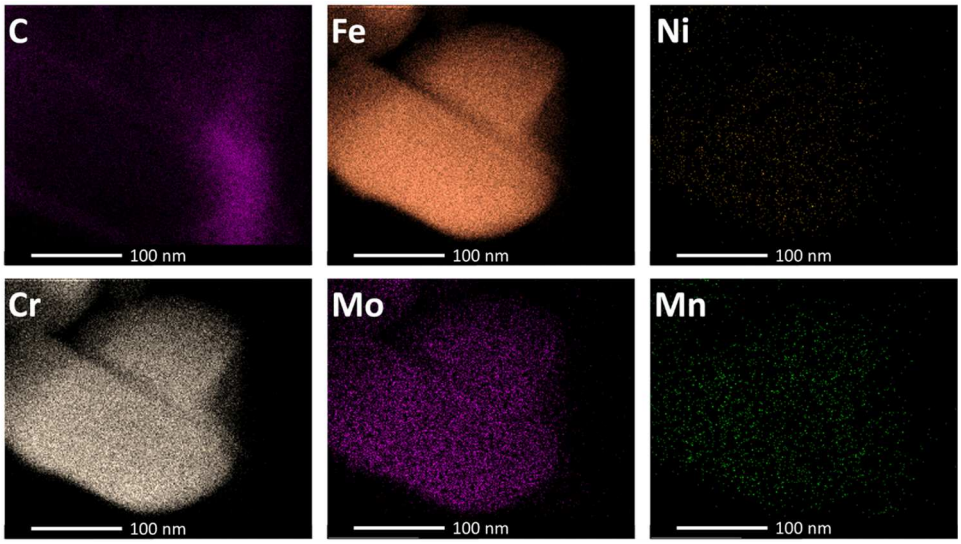

Fig. 20. EDS compositional maps in the globular base metal carbides shown in Fig. 19d.

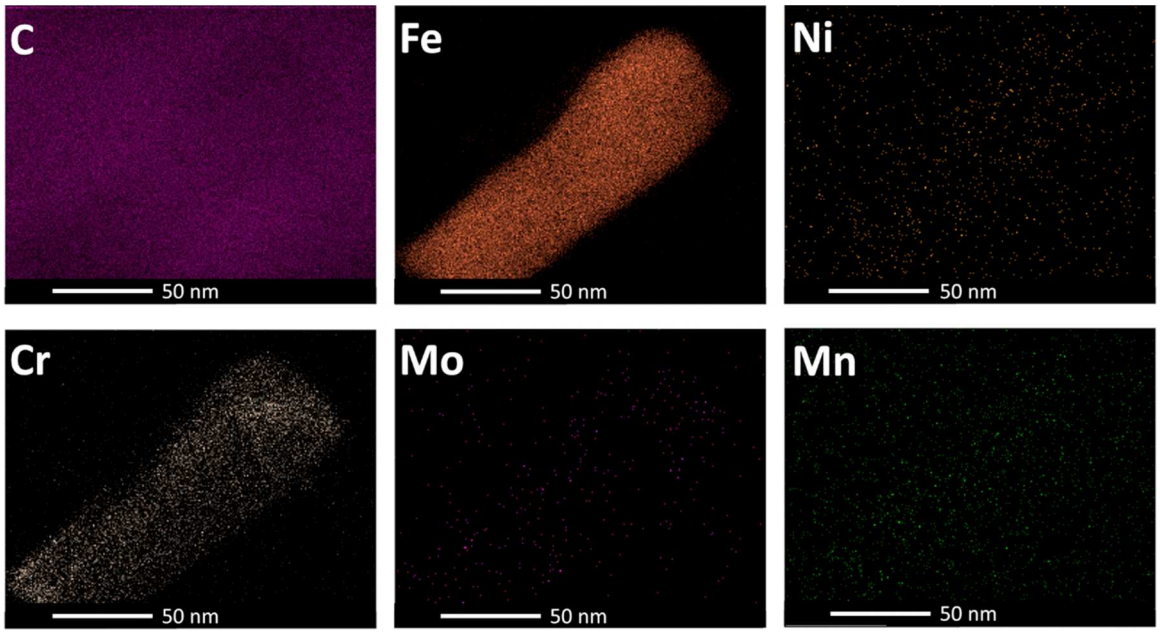

Fig. 21. EDS compositional maps in the rod-like CGHAZ carbide shown in Fig. 19e.

which utilizes a diffusion type relationship, and the hardness resulting from single and multiple tempering reheats validates the proposed tempering response quantification methodology.

5. Summary and conclusions

1 A new methodology for quantification of the tempering response in the heat affected zone of steels during welding was developed and experimentally validated. The methodology utilizes a modified Grange Baughman Parameter, which accounts for the effect of multiple non-isothermal short tempering cycles, and physical simulations of tempering to generate polynomial equations for estimation of the resulting hardness.
2 In contrast with conventional heat treatments, the tempering phenomenon in temper bead welding is characterized by heterogeneous nucleation of high density, finely dispersed Fe-Cr rich carbides. Such precipitation behavior is attributed to short-term high temperature exposures of the HAZ during temper bead welding.
3 The proposed methodology addresses the microstructural aspect of tempering, as reflected by reduction in hardness, in steels that undergo martensitic and/or bainitic transformation in the HAZ during welding.
4 In combination with computational modeling of weld thermal histories, this methodology can be used in development and optimization of efficient temper bead welding procedures. It is applicable to processes that would impart multiple short-term tempering cycles, such as additive manufacturing, spot heat treatment, and induction tempering.
5 Using the new methodology, polynomial equations for quantification of the tempering response in the intercritical and coarse-grained heat affected zones in particular heat of Grade 22 steel, resulting from single and multiple reheats, were developed.

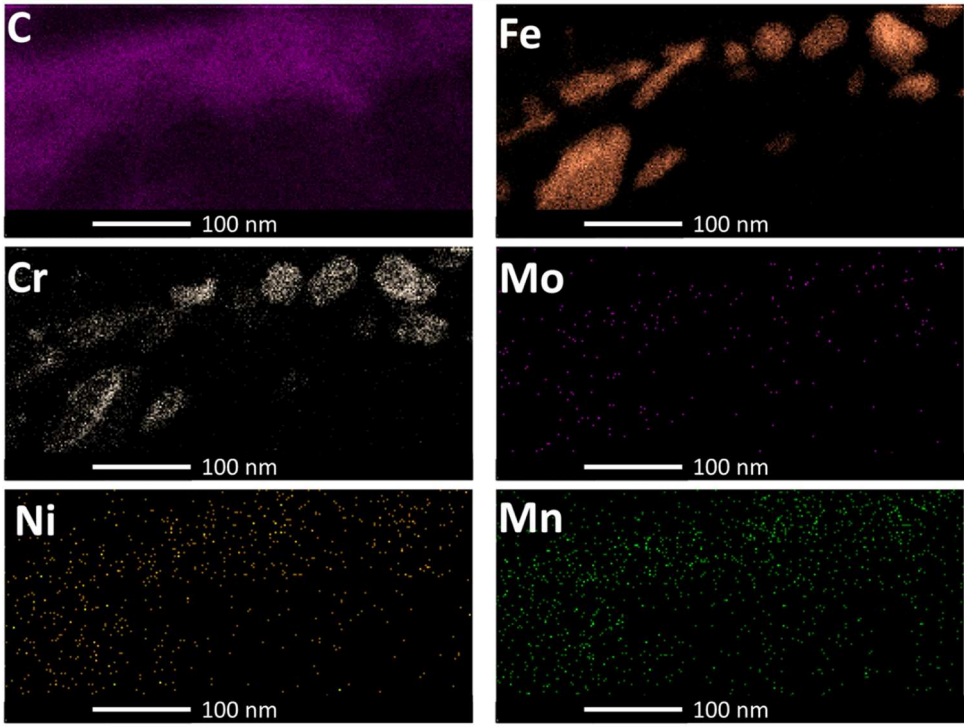

Fig. 22. EDS compositional maps in the globular CGHAZ carbides located along prior austenite gran boundary shown in Fig. 19f.

6 The physical simulations performed in this study revealed that the thermal history peak temperature is the most significant factor controlling the tempering effect of a single short-term reheat cycle. In the case of multiple reheat cycles, the tempering cycle with the highest peak temperature has the strongest tempering effect. Related to multipass welding, these results imply that weld bead overlaps in the first layer and weld beads from the second layer would have the strongest tempering effects.

7 The experimental weld overlay characterized in this study experienced significant tempering in the high temperature portion of the heat affected zone. However, the utilized welding procedure did not allow for sufficiently high tempering reheats and appreciable hardness reduction in the lower temperature portion of the head affected zone.

Declaration of Competing Interest

The authors declare that they have no known competing financial interests or personal relationships that could have appeared to influence the work reported in this paper.

Acknowledgements

This research was supported by the NSF Manufacturing and Materials Innovation Joining Center (Ma^2JIC). The authors acknowledge the guidance and advice of Mr. Steven McCracken of the Electrical Power Research Institute, Dr. Darren Barborak of AZZ Specialty Welding, Dr. Jorge Penso of Shell Global Solutions Inc., and Mr. Michael Buehner of TechnipFMC. The authors also acknowledge Mr. Hendrik Colijn of the Ohio State Center for Electron Microscopy and Analysis (CEMAS) for his assistance in obtaining and analyzing the TEM results for this study.

References

[1] Smith WF. Structure and property of engineering alloys. New York: McGraw-Hill; 1993.
[2] Porter DA, Easterling KE. Phase transformations in metals and alloys. 2nd ed. New York: Chapman & Hall; 1992.
[3] Baker RG, Nutting J. The tempering of 2.25%Cr-1%Mo steel after quenching and normalizing. J Iron Steel Inst 1959;192(3):257–68.
[4] Yu J. Carbide stability diagrams in 2.25Cr-1Mo steels. Metall Trans A 1989;20A:1561–2.
[5] Dépinoy S, Toffolon-Masclet D, Marini B. Evolution of microstructure during tempering and its influence on the mechanical behavior of 2.25Cr-1Mo bainitic steel. PTM 2015, Proc. Int. Conf. Solid-Solid Phase Transform. Inorg. Mater. 2015:1115–22.
[6] Parameswaran P, Vijayalakshmi M, Raghunathan VS. The influence of prior microstructure on tempering stages in 2.25Cr-1Mo steel. High Temp Mater Process 2002;21(5):251–67.
[7] Hollomon JH, Jaffe LD. Time-temperature relations in tempering steels. Trans AIME 1945;162:223–49.
[8] Andrews KW. Some observations on the use of a time-temperature parameter. Special Report 64. The Iron Steel Inst.; 1959. p. 292–4.
[9] Nehrenberg AE. Master curves simplify stainless tempering. Steel 1950;127:72–6.
[10] Grange RA, Baughman RW. Hardness of tempered martensite in carbon and low alloy steels. Trans ASM 1956;48:165–97.
[11] Grange RA, Hribal CR, Porter LF. Hardness of tempered martensite in carbon and low-alloy steels. Metall Trans A 1977;8A:1775–85.
[12] Semiatin SL, Stutz DE, Byrer TG. Induction tempering of steel: part I. Development of an effective tempering parameter. Htm J Heat Treat 1985;4(1):39–46.
[13] Semiatin SL, Stutz DE, Byrer TG. Induction tempering of steel: part II. Effect of process variables. Htm J Heat Treat 1985;4(1):39–46.
[14] Yu L, Nakabayashi Y, Sasa M, Itoh S, Kameyama M, Hirano S, et al. Neural network prediction of hardness in HAZ of temper bead welding using the proposed thermal cycle tempering parameter (TCTP). ISIJ Int 2011;51(9):1506–15.
[15] Yu L, Sakai T, Saida K, Nishimoto K, Sakata Y. Implementation of the quantitative evaluation method of the tempering effect during heating and cooling processes in post-weld heat treatment. Weld Int 2016;30(10):763–76.
[16] Sperko WJ. Exploring temper bead welding. Weld J 2005;84(7):37–40.
[17] Wang Y, Lundin CD, Qiao CYP, Khan KK, AI-Ejel K, Batten GW. Half-bead temper-bead controlled deposition techniques for improvement of fabrication and service performance of Cr-Mo steels. The Welding Research Council, Inc.; 2006. p. 1–251. WRC Bulletin 506.
[18] Boring MA. Development of a dissimilar temper bead welding procedure for an amine tower repair. ASME, pressure vessels and piping. paper PVP2008-61779. 2008.
[19] Peterson A. Temperbead qualification. Joint P3 weld qualification. EPRI technical report 1003292. 2002.
[20] Easterling K. Introduction to the physical metallurgy of welding. Second edition. Butterworth/ Heinemann; 1992.
[21] Hou Z, Babu RP, Hedstrom P, Odqvist J. Microstructure evolution during tempering of martensitic Fe-C-Cr alloys at 700 °C. J Mater Sci 2018;53:6063–950.